Planetesimal formation in self-gravitating discs – dust trapping by vortices

P. G. Gibbons[1]⋆, G. R. Mamatsashvili[2,3] and W. K. M. Rice[1]

[1]*SUPA, Institute for Astronomy, Royal Observatory, Blackford Hill, Edinburgh EH9 3HJ*
[2]*Department of Physics, Faculty of Exact and Natural Sciences, Tbilisi State University, Tbilisi 0179, Georgia*
[3]*Abastumani Astrophysical Observatory, Ilia State University, Tbilisi 0162, Georgia*

ABSTRACT
The mechanism through which meter-sized boulders grow to km-sized planetesimals in protoplanetary discs is a subject of active research, since it is critical for planet formation. To avoid spiralling into the protostar due to aerodynamic drag, objects must rapidly grow from cm-sized pebbles, which are tightly coupled to the gas, to large boulders of 1-100m in diameter. It is already well known that over-densities in the gaseous component of the disc provide potential sites for the collection of solids, and that significant density structures in the gaseous component of the disc (e.g., spiral density waves) can trap solids efficiently enough for the solid component of the disc to undergo further gravitational collapse due to their own self-gravity. In this work, we employ the PENCIL CODE to conduct local shearing sheet simulations of massive self-gravitating protoplanetary discs, to study the effect of anticyclonic transient vortices, or eddies, on the evolution of solids in these discs. We find that these types of structures are extremely efficient at concentrating small and intermediate-sized dust particles with friction times comparable to, or less than, the local orbital period of the disc. This can lead to significant over-densities in the solid component of the disc, with density enhancements comparable to, and even higher, than those within spiral density waves; increasing the rate of gravitational collapse of solids into bound structures.

Key words: accretion, accretion discs - gravitation - hydrodynamics - instabilities - planets and satellites: formation

1 INTRODUCTION

Large-scale spiral density waves commonly arise in a protoplanetary disc due to the gravitational instabilities at the early stage of disc life, when it is sufficiently massive. It has been known for some time that the density waves can act to transport angular momentum outwards, allowing mass to accrete onto the protostar, and could well be the primary transport mechanism provided thus by disc self-gravity during the earliest stages of star formation (e.g., Lin & Pringle 1987; Rice et al. 2010).

The other perturbation type in discs that has received much attention, partly in connection with planetesimal formation, are vortices. They can arise in both self-gravitating and non-self-gravitating discs by several means. A localized radial structure in the disc can trigger the Rossby wave instability, which in turn results in the formation of vortices (e.g., Lovelace et al. 1999; Li et al. 2000; Lyra et al. 2009; Meheut et al. 2010, 2012a; Lin 2012a; Regaly et al.

2012). Vortices can also be generated as a result of other hydrodynamic instabilities, such as the baroclinic instability (Klahr & Bodenheimer 2003; Petersen et al. 2007; Lesur & Papaloizou 2010; Raettig et al. 2013) or the Kelvin-Helmholtz instability of seed vorticity strips (Lithwick 2007). Although the dynamics and evolution of vortices in non-self-gravitating discs has been under active investigation for a while, since the first idea of their relevance to planet formation by Barge & Sommeria (1995), systematic studies of vortex dynamics in self-gravitating discs are quite recent (Mamatsashvili & Rice 2009; Lyra et al. 2009; Lin 2012b; Lovelace & Hohlfeld 2013; Ataiee et al. 2014). It was commonly thought that spiral density waves are the only perturbation type present in self-gravitating discs, and the existence of other modes also participating in the overall disc dynamics had been ignored in many studies of self-gravitating discs.

Developments in the theory of non-self-gravitating discs, however, showed that vortices can be (linearly) coupled with, and excite, spiral density waves due to the disc's differential rotation (Bodo et al. 2005; Johnson & Gammie

⋆ E-mail: pgg@roe.ac.uk

2005; Heinemann & Papaloizou 2009). This effect was demonstrated to be even more efficient in the presence of self-gravity (Mamatsashvili & Chagelishvili 2007). Moreover, a linear analysis by Mamatsashvili & Chagelishvili (2007) showed that in fact vortical mode is also subject to the influence of self-gravity and can exhibit gravitational instability with amplification factors comparable to that of density waves. This clearly implies that vortices are as important as density waves in forming a complete dynamical picture of self-gravitating discs.

Subsequent nonlinear dynamics and evolution of vortices varies greatly in non-self-gravitating and self-gravitating systems. In non-self-gravitating discs, small-scale (anticyclonic) vortices, soon after formation, smoothly merge into each other and increase in size (e.g., Li et al. 2001; Godon & Livio 1999, 2000; Klahr & Bodenheimer 2003; Umurhan & Regev 2004; Johnson & Gammie 2005; Shen et al. 2006). When the vortices reach a few scale height, compressibility becomes important, causing them to emit spiral density waves - due to the above-mentioned mode coupling phenomenon - and, consequently, slowly decay on the time-scale of several hundred orbital periods (Johnson & Gammie 2005; Shen et al. 2006; Bodo et al. 2007). In spite of this shock dissipation, anticyclonic vortices can be considered long-lived, coherent structures in discs. However, they can be subject to radial migration (Paardekooper et al. 2010) and/or to the elliptical instability (Lesur & Papaloizou 2009; Richard et al. 2013), the typical time-scale of which is larger than vortex turnover/orbital time, as well as to destruction by the magnetorotational instability in magnetized regions (Lyra & Klahr 2011).

The vortex merging is resisted under the influence of disc self-gravity and smaller size vortices are favoured (Mamatsashvili & Rice 2009; Lyra et al. 2009; Lin 2012b). In some sense, self-gravity acts to oppose the inverse cascade of spectral energy to larger scales, as occurs in the non-self-gravitating case, and, instead, scatters it to smaller scales. The local shearing sheet simulations of radially un-structured (i.e., in the absence of baroclinic or Rossby wave instabilities) discs by Mamatsashvili & Rice (2009) demonstrate that vortices in a quasi-steady gravitoturbulence are transient, short-lived structures undergoing repeating cycles of formation, growth to sizes comparable to the local Jeans length, and eventual shearing and destruction due to the effects of self-gravity and Keplerian shear. This process lasts a few orbital periods, and results in a very different, compared to the non-self-gravitating case, evolutionary picture, with many small, less organized vortices (eddies) in various stages of evolution, rather than the relatively larger scale well organized vortices gradually growing via slow mergers. On the other hand, in global simulations by Lyra et al. (2009); Lin (2012b) discs are radially structured and, although they remain laminar (without gravitoturbulence), develop vortices via Rossby wave instability at vortensity minimum. Due to self-gravity, these vortices have a smaller azimuthal extent (i.e., higher azimuthal wavenumbers) compared with similar ones without self-gravity. What is noteworthy, however, vortices in both local and global simulations share a common feature – they produce over-densities at their centres coinciding with the minima of Toomre's parameter Q. These over-densities are imposed on the density variations due to shocks of density waves emitted by these vortices.

In massive discs, the gravitational instabilities have been shown to cause the disc to fragment, possibly leading to the direct formation of gas giant planets (Boss 1998; Gammie 2001; Rice et al. 2003; Paardekooper 2012). Although a massive protoplanetary disc is thought to be present at early times in the star formation process, it is not clear that such discs can cool fast enough due to radiative transfer to directly form giant planets via this mechanism (Rafikov 2005; Boley et al. 2006; Clarke 2009; Rice & Armitage 2009). However, even if the effective cooling times present within discs are too long to allow giant planets to form via fragmentation, as mentioned above, protoplanetary discs are very likely self-gravitating in their early stages (Lin & Pringle 1987, 1990), sometimes even at the T Tauri stage (Eisner et al. 2005; Andrews & Williams 2007). In this case, indirect means of planet formation – accumulation of dust particles in gaseous density structures that arise as a result of the gravitational instability – could be at work. As outlined above, such structures can be either due to density waves or to smaller scale vortices.

In low mass discs, where self-gravity is negligible, vortices have been shown to have a significant influence on the local evolution of dust particles (e.g., Johansen et al. 2004; Klahr & Bodenheimer 2006; Meheut et al. 2012b; Lyra & Lin 2013; Fu et al. 2014; Zhu et al. 2014). In these simulations, not including self-gravity, dust grains with a wide range of sizes were shown to be trapped within the centres of the vortex structures with the strongest concentration occurring for particles with friction/stopping times comparable to the local orbital period. In other words, a smooth, sufficiently long-lived vortex is indeed able to effectively trap dust particles in its core, possibly accelerating planetesimal formation.

To date, however, the evolution of dust particles in self-gravitating discs has been primarily studied in a large scale setting, concentrating on the effect spiral density waves, in the gaseous component of the disc, have on dust particles. Rice et al. (2004, 2006) used global simulations to show that the presence of spiral density waves in the disc can have a dramatic effect on the particle layer. In Rice et al. (2004), the dust particles are assumed to interact with the disc solely via an aerodynamic drag force. The particles, especially those with stopping times comparable to the local orbital period, are shown to become trapped within the density wave structures that form in the disc due to self-gravity. This causes the local density of solid material within the density waves to rise by an order of magnitude or more compared to the average. The gas pressure gradient changes from positive to negative across the density wave structure, creating sub-Keplerian velocities on one side of the wave, and super-Keplerian on the other. As a result, the drag force causes dust grains to drift toward the density/pressure maxima at the crest of density waves.

Rice et al. (2006) generalized these findings by including the gravitational effects of the solid particles themselves, which allow these particle enhancements to become even more pronounced, resulting in gravitationally bound clumps, or planetesimals, forming in the disc. More recently, these results were expanded on in Gibbons et al. (2012, 2014) using higher resolution two-dimensional (2D) local shearing sheet simulations of self-gravitating gaseous discs, treated as in related local studies (Gammie 2001; Rice et al. 2011;

Paardekooper 2012), with added numerical super-particles to model dust-particle dynamics. These studies found that the spiral density waves are very efficient at trapping relatively small, from several centimeter up to meter-sized particles, whose stopping times are comparable to the local orbital period. Very tightly bound clumps of particles can form in the crests of these spiral waves due to the strong gravitational attraction between particles at such high concentrations. These processes can result in a substantial population of large, planetesimal-sized solid objects being rapidly formed in the early stages of disc evolution, paving the way for terrestrial and gas giant planet formation via the traditional core-accretion model (e.g., Pollack et al. 1996).

Dust particles can also become trapped by pressure maxima associated with (anticyclonic) vortices and, as mentioned above, this process has been extensively studied in non-self-gravitating discs. The role of vortices in trapping dust in self-gravitating discs is less understood and needs further investigation, because of the different character of vortex evolution with self-gravity. Particle concentration by vortices, as well as vortex dynamics itself in the presence of self-gravity, was first addressed by Lyra et al. (2009) via global disc simulations. However, in their set-up vortices are generated by the Rossby wave instability in an otherwise laminar disc and have a long-lived regular nature - as in the non-self-gravitating case - though smaller azimuthal size due to the effect of self-gravity. Here, we consider a different situation – a self-gravitating disc in a quasi-steady gravitoturbulent state, without continuous driving by global baroclinic or Rossby wave instabilities, and analyse the behaviour of embedded dust particles using the shearing sheet approximation. We would like to note that on shorter (comparable to the disc scale height or less) length-scales just such a gravitoturbulent state, rather than a regular/coherent one, is more common in self-gravitating discs (e.g., Gammie 2001; Durisen et al. 2007). As shown by Mamatsashvili & Rice (2009), this state consists of transient short-lived small-scale vortices producing over-dense regions overlaid on density wave structures. In other words, we extend this study by including dust particles with a goal of understanding the role these vortical structures play in dust evolution. Dust dynamics in the presence of only density waves in the shearing sheet has been explored in our previous papers (Gibbons et al. 2012, 2014), where larger domain sizes were used. Here, we take a smaller size domain that enables us to zoom in on smaller scale vortical structures and examine their dust trapping capability against the backdrop of density variations due to the density waves (shocks). This will help us to establish the role of vortices in planet formation process in self-gravitating discs.

The paper is organized as follows. In Section 2, we outline the physical set-up and initial conditions adopted in our simulations. In Section 3, we discuss the evolution of the dust particles in the the vortex structures in the gas. Finally, summary and discussions are given in Section 4.

2 MODEL

To investigate the dynamics of solid particles embedded in a self-gravitating protoplanetary disc, we solve the 2D local shearing sheet equations for gas on a fixed grid, including disc self-gravity, together with the equations of motion of solid particles coupled to the gas through aerodynamic drag force. We also include the self-gravity of particles necessary to examine their collapse properties. As a main numerical tool, we employ the PENCIL CODE [1]. It is a sixth order spatial and third order temporal finite difference code (see Brandenburg (2003) for full details). The PENCIL CODE treats solids as numerical super-particles (Johansen et al. 2006, 2011).

In the shearing sheet approximation, disc dynamics is studied in the local Cartesian coordinate frame centred at some fiducial radius, r_0, from the central object, and rotating with the disc's angular frequency, Ω, at this radius. In this frame with the x-and $y-$axis pointing, respectively, in the radial and azimuthal directions, the disc's differential rotation manifests itself as an azimuthal parallel flow characterized by a linear shear, q, of background velocity along the $x-$axis, $\mathbf{u}_0 = (0, -q\Omega x)$. The equilibrium surface densities of gas, Σ_0, and particles, Σ_{p0}, are spatially uniform. Since the disc is cool, and therefore thin, the aspect ratio is small, $H/r_0 \ll 1$, where $H = c_s/\Omega$ is the disc scale height, and c_s is the gas sound speed. The local shearing sheet model is based on the expansion of the basic 2D hydrodynamic equations of motion to the lowest order in this small parameter, assuming that the disc is razor thin (see e.g., Gammie 2001).

Our simulation domain spans the region $-L_x/2 \leqslant x \leqslant L_x/2$, $-L_y/2 \leqslant y \leqslant L_y/2$. As is customary, we adopt the standard shear-periodic boundary conditions well approbated in shearing sheet studies of discs (e.g., Gammie 2001; Johansen & Youdin 2007). Namely, for any variable f, including azimuthal velocity with background flow subtracted, we have

$$f(x,y,t) = f(x + L_x, y - q\Omega L_x t, t), \qquad (x - \text{boundary})$$

$$f(x,y,t) = f(x, y + L_y, t), \qquad (y - \text{boundary})$$

The shear parameter is $q = 1.5$ for the Keplerian rotation profile adopted in this paper.

2.1 Gas density

In this local model, the continuity equation for the vertically integrated gas density Σ is

$$\frac{\partial \Sigma}{\partial t} + \nabla \cdot (\Sigma \mathbf{u}) - q\Omega x \frac{\partial \Sigma}{\partial y} - f_D(\Sigma) = 0 \qquad (1)$$

where $\mathbf{u} = (u_x, u_y)$ is the gas velocity relative to the background Keplerian shear flow $\mathbf{u}_0$. Due to the high-order numerical scheme of the PENCIL CODE it also includes a diffusion term, f_D, to ensure numerical stability and capture shocks,

$$f_D = \zeta_D(\nabla^2 \Sigma + \nabla \ln \zeta_D \cdot \nabla \Sigma).$$

Here the quantity ζ_D is the shock diffusion coefficient defined as

$$\zeta_D = D_{sh} \langle \max_3[(-\nabla \cdot \mathbf{u})_+] \rangle (\delta x)^2$$

---

[1] See http://code.google.com/p/pencil-code/

where D_{sh} is a constant, characterizing the strength of shock diffusion as outlined in Appendix B of Lyra et al. (2008), and $\delta x = L_x/N_x$ is the grid cell size.

2.2 Gas velocity

The equation of motion for the gas relative to the unperturbed Keplerian flow takes the form

$$\frac{\partial \mathbf{u}}{\partial t} + (\mathbf{u} \cdot \nabla)\mathbf{u} - q\Omega x \frac{\partial \mathbf{u}}{\partial y} = -\frac{\nabla P}{\Sigma} - 2\Omega \hat{\mathbf{z}} \times \mathbf{u} + q\Omega u_x \hat{\mathbf{y}}$$
$$- \frac{\Sigma_p}{\Sigma} \cdot \frac{\mathbf{u} - \mathbf{v}_p}{\tau_f} - \nabla \psi + \mathbf{f}_\nu(\mathbf{u}), \quad (2)$$

where P is the vertically integrated pressure, Σ_p is the surface density of particles, ψ is the gravitational potential produced jointly by the gas and particle surface densities (see equation 6). The left hand side of equation (2) describes the advection by the velocity field, $\mathbf{u}$, itself and by the mean Keplerian flow. On the right hand side, the first term is the pressure force, the second and third terms represent the Coriolis force and the effect of shear, respectively, and the fourth term describes the back-reaction exerted on the gas by the dust particles due to aerodynamic drag force (see e.g., Lyra et al. 2009; Johansen et al. 2011). This force is proportional to Σ_p and to the difference between the velocity of particles $\mathbf{v}_p$ and the gas velocity $\mathbf{u}$ and is inversely proportional to the stopping, or friction time, τ_f, of particles. The fifth term represents the force due to self-gravity of the system. Finally, the code includes an explicit viscosity term, $\mathbf{f}_\nu$,

$$\mathbf{f}_\nu = \nu(\nabla^2 \mathbf{u} + \frac{1}{3}\nabla\nabla \cdot \mathbf{u} + 2\mathbf{S} \cdot \nabla\ln \Sigma)$$
$$+ \zeta_\nu[\nabla(\nabla \cdot \mathbf{u}) + (\nabla\ln \Sigma + \nabla\ln \zeta_\nu)\nabla \cdot \mathbf{u}],$$

which contains both shear viscosity and a bulk viscosity for resolving shocks. Here $\mathbf{S}$ is the traceless rate-of-strain tensor

$$S_{ij} = \frac{1}{2}\left(\frac{\partial u_i}{\partial x_j} + \frac{\partial u_j}{\partial x_i} - \frac{2}{3}\delta_{ij}\nabla \cdot \mathbf{u}\right)$$

and ζ_ν is the shock viscosity coefficient analogous to the shock diffusion coefficient ζ_D defined above, but with D_{sh} replaced by ν_{sh}.

2.3 Entropy

The PENCIL CODE uses entropy, s, as its main thermodynamic variable, rather than internal energy, U. The equation for entropy evolution is

$$\frac{\partial s}{\partial t} + (\mathbf{u} \cdot \nabla)s - q\Omega x \frac{\partial s}{\partial y} = \frac{1}{\Sigma T}\left(2\Sigma\nu\mathbf{S}^2 - \frac{\Sigma c_s^2}{\gamma(\gamma-1)t_c} + f_\chi(s)\right) \quad (3)$$

where the first term on the right hand side is the viscous heating term and the second term is an explicit cooling. Following Gammie (2001); Rice et al. (2011); Paardekooper (2012), we assume the effective cooling time t_c to be constant throughout the simulation domain and take its value $t_c = 20\Omega^{-1}$, which is sufficiently large for the disc to avoid fragmentation and settle into a quasi-steady self-regulated state. The final term on the right hand side, $f_\chi(s)$, is a shock dissipation term analogous to that outlined for the density.

2.4 Dust particles

The dust particles are treated as a large number of numerical super-particles (Johansen et al. 2011) with positions $\mathbf{r}_p = (x_p, y_p)$ on the grid and velocities $\mathbf{v}_p = (v_{p,x}, v_{p,y})$ relative to the unperturbed Keplerian rotation velocity, $\mathbf{v}_{p,0} = (0, -q\Omega x_p)$, of particles in the local Cartesian frame. These are evolved according to

$$\frac{d\mathbf{r}_p}{dt} = \mathbf{v}_p - q\Omega x_p\hat{\mathbf{y}} \quad (4)$$

$$\frac{d\mathbf{v}_p}{dt} = -2\Omega\hat{\mathbf{z}} \times \mathbf{v}_p + q\Omega v_{p,x}\hat{\mathbf{y}} - \nabla\psi + \frac{\mathbf{u} - \mathbf{v}_p}{\tau_f}. \quad (5)$$

The first two terms on the right hand side of equation (5) represent the Coriolis force and the non-inertial force due to shear. The third term is the force exerted on the particles due to the common gravitational potential ψ. The fourth term describes the drag force exerted by the gas on the particles which arises from the velocity difference between the two. Unlike the gas, the particles do not feel the pressure force. In the code, the drag force on the particles from the gas is calculated by interpolating the gas velocity field to the position of the particle, using the second order spline interpolation outlined in Appendix A of Youdin & Johansen (2007). The back-reaction on the gas from particles in equation (2) is calculated by the scheme outlined in Johansen et al. (2011).

2.5 Self-gravity

The gravitational potential in the dynamical equations (2) and (5) is calculated by inverting Poisson equation for it, which contains on the right hand side the gas plus particle surface densities in a razor thin disc (e.g., Lyra et al. 2009)

$$\Delta\psi = 4\pi G(\Sigma - \Sigma_0 + \Sigma_p - \Sigma_{p0})\delta(z) \quad (6)$$

using the Fast Fourier Transform (FFT) method outlined in the supplementary material of Johansen et al. (2007). Note that the perturbed gas, $\Sigma - \Sigma_0$, and particle, $\Sigma_p - \Sigma_{p0}$, surface densities enter equation (6), since only the gravitational potential associated with the perturbed motion (and hence density perturbation) of both the gaseous and solid components determine gravity force in equations (2) and (5). Here, the surface density is Fourier transformed from the (x, y)-plane to the (k_x, k_y)-plane without the intermediate co-ordinate transformation performed by Gammie (2001). For this purpose, a standard FFT method has been adapted to allow for the fact that the radial wavenumber k_x of each spatial Fourier harmonic depends on time as $k_x(t) = k_x(0) + q\Omega k_y t$ in order to satisfy the shearing sheet boundary conditions (see also Mamatsashvili & Rice 2009).

2.6 Units and Initial Conditions

We normalise the quantities by setting $c_{s0} = \Omega = \Sigma_0 = 1$. The time and velocity units are $[t] = \Omega^{-1}$ and $[v] = c_{s0}$, resulting in the orbital period, $T_{orb} = 2\pi$. The unit of length is the scale height, $[l] = H = c_{s0}/\Omega$. The initial Toomre parameter $Q = c_{s0}\Omega/\pi G\Sigma_0$ is equal to 1 throughout the domain. This sets the gravitational constant $G = \pi^{-1}$. The surface density of gas is initially set to unity everywhere in
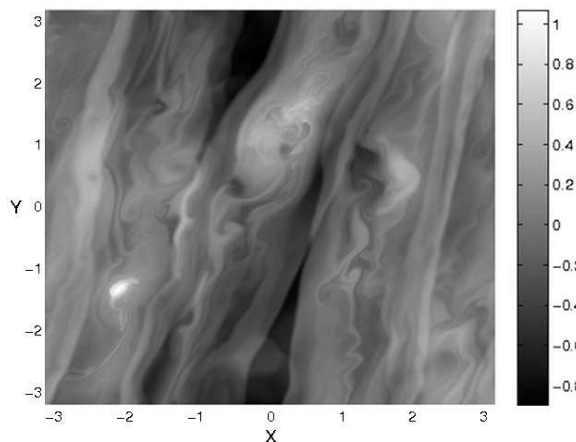
Figure 1. Logarithmic surface density of the gas after 40 orbits, just before the self-gravity of the particles is introduced. The disc has already settled into a quasi-steady gravitoturbulent state. Superimposed on the larger scale density waves are the smaller scale over-dense structures due to irregular vortices (see Fig. 2). The distribution of dust particles at the same time is shown in Fig. 3.

Figure 2. PV field, I, in the quasi-steady state at the same time as in Fig. 1. Numerous small-scale, irregularly shaped, anticyclonic vortices (eddies), corresponding to negative PV regions (black dots and curly diffuse areas) have developed in the sheet. The over-dense structures produced by these vortices are clearly seen in the gas density field shown in Fig. 1. The colour-map is restricted to the range $-20 \leqslant I \leqslant 20$ to better emphasize/visualize the presence of the vortical structures.

the sheet. The simulation domain is a square with dimensions $L_x = L_y = 20G\Sigma_0/\Omega^2$ and is divided into a grid of $N_x \times N_y = 1024 \times 1024$ cells. This choice of units sets the domain length $L_x = 20H/\pi Q \approx 6.37H$ and the corresponding grid cell size $\delta x = \delta y = 0.0062H$.

The gas velocity field is initially perturbed by some small random fluctuations with the rms amplitude $\sqrt{\langle \mathbf{u}^2 \rangle} = 10^{-3}$. We take the viscosity and diffusion coefficients to be $\nu = 10^{-4}$ and $\nu_{sh} = D_{sh} = 10.0$, this ensures numerical stability across the shock fronts, without washing them out. We use 10^6 particles, split evenly between five friction times, $\tau_f = [0.01, 0.1, 1, 10, 100]\Omega^{-1}$. The dust particles are initially randomly placed throughout the domain with zero velocity and do not interact with the gas or other dust particles for the first 10 orbital periods. At this point, once the gas has settled into a quasi-steady state, which is independent of its initial conditions, the drag forces between the dust particles and gas are introduced. The system is then evolved for a further 30 orbits, before the particles' self-gravity is introduced. The initial value for the dust-to-gas surface density ratio, Σ_{p0}/Σ_0, is taken to be 0.01 for each particle species.

3   RESULTS

3.1   Gas Evolution

The evolution of the gaseous component of the disc is in good agreement with that observed in previous analogous studies of self-gravitating discs in the shearing sheet with an imposed constant cooling time. The initial perturbations grow and develop into nonlinear fluctuations in velocity, surface density and potential. Shocks then form, which proceed to heat the gas, while the cooling acts to reduce the internal energy and entropy of the gas. Density structures develop, which are sheared out by differential rotation. Once the system has completed several orbits, the heating generated by the shocks is balanced by the cooling term, and the system settles into a quasi-steady, self-regulated state. In
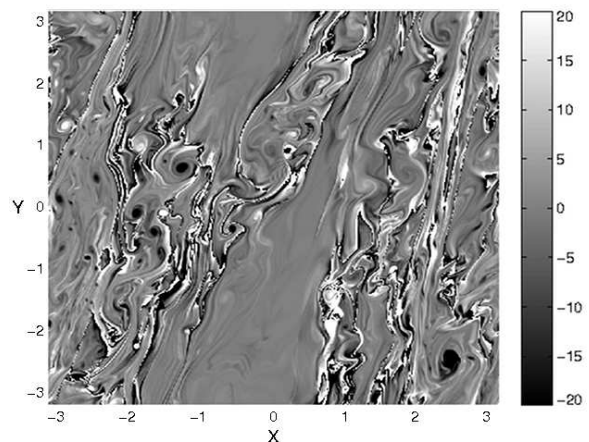
this gravitoturbulent state, the thermal, kinetic and gravitational energies of the disc are on average constant over time. The saturated value of the shear stress parameter α is proportional to the inverse cooling time, while the amplitude of the density fluctuations to the square root of the inverse cooling time (Cossins et al. 2009; Rice et al. 2011). Figure 1 shows the surface density of the gas after 40 orbits in the fully developed quasi-steady gravitoturbulence. Here, the large-scale shocks due to density waves are visible along with the smaller scale structures associated with vortices.[2] The dynamics of these vortices in the gravitoturbulent state was investigated by Mamatsashvili & Rice (2009), which we recap below.

The vortical structures in the gas are characterized by the potential vorticity (PV),

$$I \equiv \frac{(\nabla \times \mathbf{u}) \cdot \hat{\mathbf{z}} + (2 - q)\Omega}{\Sigma}.$$

During the burst phase, initial small-scale positive and negative PV regions are strongly sheared into strips, but negative PV (anticyclonic) regions start to wrap up into vortex-like structures due to the nonlinear Kelvin-Helmholtz instability (Lithwick 2007). The positive PV regions remain sheared into strips, showing no signs of vortex formation during the entire course of evolution. Only these anticyclonic regions, having negative PV, are able to survive in the flow by taking the form of vortices, though they are not as regular/coherent as those occurring in non-self-gravitating discs (e.g., Umurhan & Regev 2004; Johnson & Gammie 2005; Shen et al. 2006). These smaller scale, irregular anticyclonic vortices, or eddies, characterized by negative PV, which have

---

[2] In the Appendix, we show, by calculating the autocorrelation function for the PV field in the quasi-steady state, that the shortest correlation length for these vortices is more than 10 times larger than the grid cell size, implying that they are sufficiently resolved in our simulations.

developed in the quasi-steady state are clearly seen in the PV field in Fig. 2. They induce spatial variations (structures) with a similar form in the gas surface density due to compressibility and self-gravity, as clearly seen in Fig. 1. One can say that in the presence of self-gravity, the PV field makes its "imprint" in the density field. This is in contrast to the case with multiple nonlinearly interacting vortices in the non-self-gravitating shearing sheet, where only density waves (shocks) shed by them are seen in the gas density field (Shen et al. 2006). Comparing Figs. 1 and 2, we notice that those vortices with smaller, by absolute value, PV give rise to higher over-densities than those with larger, by absolute value, PV (for example, small white region in the surface density map near the lower left corner). These over-densities at some locations are even larger than the density variations near the shock fronts.

In this quasi-steady gravitoturbulent state, the vortices are transient/unsteady structures undergoing recurring phases of formation, growth to sizes comparable to a local Jeans scale and eventual shearing and destruction due to the combined effects of self-gravity (gravitational instability) and background Keplerian shear. Each phase typically lasts about two orbital periods or less. As a result, in self-gravitating discs, the overall dynamical picture of vortex evolution is irregular consisting of many transient vortices at different evolutionary stages and, therefore, with various sizes up to the local Jeans scale. By contrast, in the non-self-gravitating case, long-lived vortex structures persist for hundreds of orbits via merging of smaller vortices into larger ones until eventually their size reaches the disc scale height.

It should be noted that the disc cooling, which we have described using a simple constant cooling time prescription, in reality is due to radiative losses from the disc and depends on its physical properties (e.g., Johnson & Gammie 2003; Rafikov 2005). Obviously, cooling affects disc thermodynamics, which, in turn, through the baroclinic source, determines vortex (potential vorticity) dynamics. However, in the presence of self-gravity the situation is somewhat different. In the case of a constant cooling time, despite being a simple approximation, the disc settles into the quasi-steady gravitoturbulent state characterized by a local balance between heating and cooling, which is qualitatively similar to that with a more realistic radiative cooling (e.g., Johnson & Gammie 2003; Boley et al. 2006; Forgan et al. 2011). So, it is expected that the evolution of PV in the presence of realistic cooling will also be similar to that with a constant cooling time as long as the disc resides in the quasi-steady state and the global baroclinic or Rossby wave instabilities do not intervene in the dynamics.

In non-self-gravitating discs, regular and long-lived anticyclonic vortices have been shown to be efficient at trapping dust particles in their cores (e.g., Johansen et al. 2004; Meheut et al. 2012b; Fu et al. 2014; Zhu et al. 2014). In Section 3.2 we examine the particle trapping capabilities of these unsteady and irregular anticyclonic vortices.

3.2   Particle Concentration

Once the gas has reached a quasi-steady gravitoturbulent state, the aerodynamic drag force and the corresponding back-reaction terms are introduced into the particle and gas evolution, respectively. The simulation is then evolved for a further 30 orbits, at which time the particles have basically also settled into a quasi-steady state. The particle self-gravity is then introduced and the simulation was evolved for another 6 orbits. After this point, the high particle densities achieved in bound clumps (see below) result in the self-gravity term becoming dominant in the particle momentum equation. Consequently, the time step of the simulation becomes very small such that it is impractical to evolve the particles further. However, inspection of the particle density field up to this point indicates that the particles have been sufficiently evolved to draw some conclusions about their further behaviour. At this time, particle dynamics is practically no longer affected by gas and one must also incorporate particle collisions, which become more significant at high particle concentrations within each clump, to correctly follow the subsequent dynamics and contraction of the latter (Johansen et al. 2012).

The surface density of the particles at the end of the run with only the drag force (i.e., before introducing particle self-gravity) is plotted in Fig. 3. As shown in Gibbons et al. (2012, 2014), the small- and intermediate-sized particles with friction times $\tau_f = [0.01, 0.1, 1.0]\Omega^{-1}$ are efficiently trapped in the density wave structures in the gas, with the particles of stopping times $\tau_f = 1.0\Omega^{-1}$ exhibiting the highest concentration. Of particular interest for the present work is the behaviour of the dust particles in the vicinity of smaller scale vortices that form in and around the density wave structures. The dynamical behaviour of particles in the vicinity of these anticyclonic vortices appears to depend on their stopping time, τ_f. The particles with $\tau_f = [0.01, 0.1]\Omega^{-1}$ tend to accumulate around the central region of anticyclonic vortices, but do not drift further into their centres, leaving noticeable voids at the centres, which correspond to the local minima of PV (Fig. 2). These particles in fact trace out the over-dense structures around vortices, which, as a result, appear to be surrounded by a spiral, or ring, of dust particles. These rings also tend to contain some of the highest concentrations of particles in the domain, though not significantly larger than the concentrations found in the crests of density waves. Thus, the smaller particles with $\tau_f = [0.01, 0.1]\Omega^{-1}$ preferentially map out the vortical structures. On the other hand, the intermediate-sized particles with friction times $\tau_f = 1.0\Omega^{-1}$ get trapped into crests of density waves and even more in negative PV regions with relatively low by absolute value PV (curly areas in Fig. 2), which produce higher over-densities in the gas (Fig. 1). As opposed to the smaller friction time case, these particles fill the central parts of over-dense regions and do not leave voids. The larger particles with $\tau_f = [10.0, 100.0]\Omega^{-1}$ accumulate only in density wave crests; vortices do not seem to affect their motion, as is clear from the surface density of these particles.

This differential concentration of particles in the vortical structures depending on their friction time can be explained as follows. As described above, these small-scale vortices are transient structures, which undergo cycles of formation, amplification and shearing away over a few orbits (Mamatsashvili & Rice 2009). The small particles, with friction times less than the orbital time, are tightly coupled to the gas and therefore closely follow the density variations induced by vortices. During short times, these transient vortices are approximately in balance by self-gravity, pressure
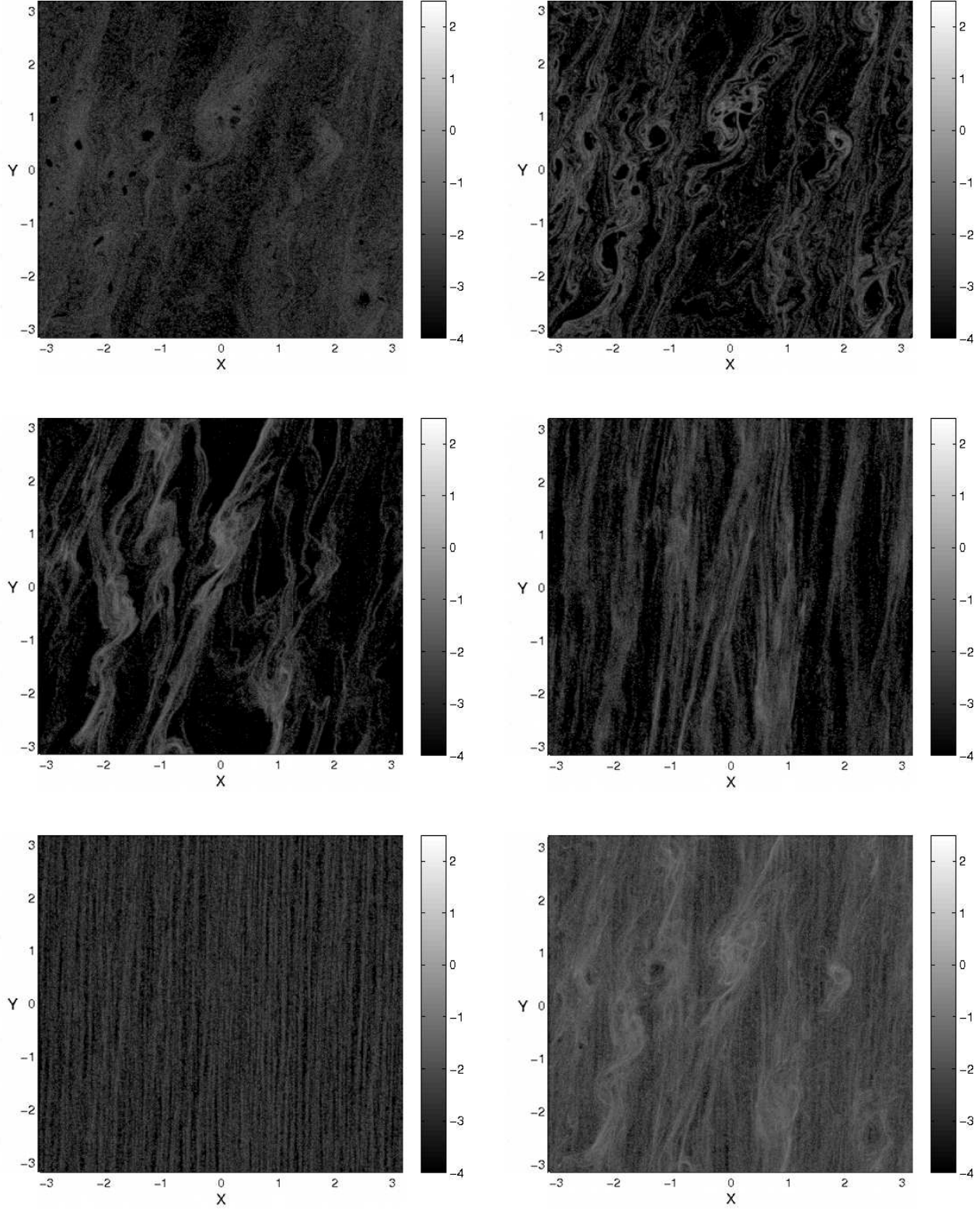
Figure 3. Logarithmic surface density of the individual dust particle species (in units of its mean $\langle \Sigma_p \rangle = \Sigma_{p0}$) after 30 orbits since the drag force between the gas and particles was introduced. The smallest particles (with $\tau_f = 0.01\Omega^{-1}$) are shown in the top left panel and the other panels, corresponding to increasing friction times, follow in lexicographic order with the largest particles (with $\tau_f = 100\Omega^{-1}$) in the bottom left panel. The total surface density of the dust is shown in the bottom right panel. For comparison, the surface density of the gas at this time is shown in Fig. 1 and the corresponding PV field is shown in Fig. 2. We observe that large particles with $\tau_f = [10, 100]\Omega^{-1}$ are accumulated in density wave crests; intermediate-sized particles with $\tau_f = 1.0\Omega^{-1}$ are captured effectively in crests of density waves and in the irregularly-shaped anticyclonic vortices, whilst the small particles with $\tau_f = [0.01, 0.1]\Omega^{-1}$ tend to preferentially accumulate around anticyclonic vortices but do not fill their central regions, as indicated by black voids, and trace out their structure (see Fig. 2).
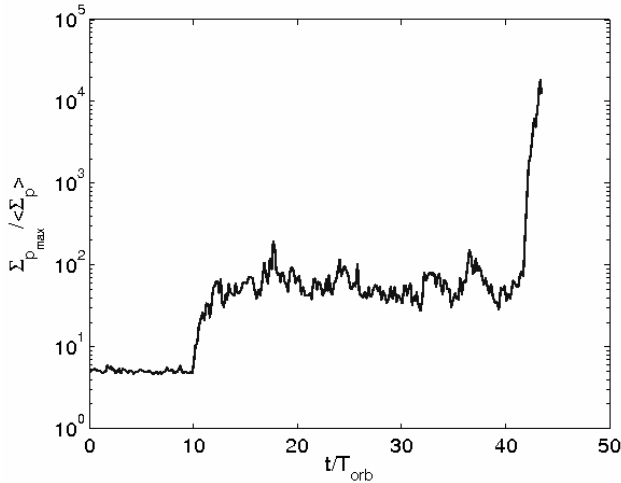
Figure 4. Maximum surface density of the particles within the domain as a function of time. The jump in the density at $t = 10T_{orb}$ corresponds to the introduction of the drag force between the gas and dust particles, whilst the second jump indicates the introduction of the particle self-gravity.

and rotation, forming under-dense core, coinciding with the minimum of PV, surrounded by over-dense ring. As a result, the small particles, rapidly adjusting to the vortical motions, get mostly concentrated in these over-dense rings, leaving the vortex centre practically empty. On the other hand, during orbital time the vortices evolve, their PV reduces by absolute value and the corresponding over-density becomes stronger and no longer has an under-dense core. The particles with friction times comparable to the orbital time tend to accumulate in these over-densities repeating their shape, though with a little delay. Larger particles are not affected by these transient vortices, because their friction times are longer than the orbital time – the characteristic time-scale of vortices.

Figure 4 shows the evolution of the maximum surface density (relative to the mean) of solids in the simulation domain. When the drag force between the particles and the gas is introduced after 10 orbits, the maximum surface density rapidly jumps, increasing by a factor of ~ 10, from a few times to almost 100 times the mean over the course of a few orbits. Then, the particles remain in a quasi-steady state, where they are trapped in vortices and/or density waves, but these gaseous structures get continuously sheared away and reappear again over few orbital times, so the particles leaving a gaseous perturbation are swept up by next one and so on. This cycle continues until the self-gravity of the particles is introduced after 40 orbits. At this point, the particle concentrations with large enough densities that have formed before this time start to undergo rapid gravitational collapse, forming many gravitationally bound clumps of particles, which undergo further mergers. The largest of these objects exhibit local surface densities thousands of times the mean surface density. These objects are sufficiently stable to remain bound after the parent density wave and/or vortical perturbation they formed in had been sheared away. The boundedness of the clumps is established by calculating total, kinetic plus gravitational energies inside an individual clump and, if the latter is negative, the clump is

classified as gravitationally bound. The map of the surface density of the solids at the end of the simulation is shown in Fig. 5, where we clearly see bound clumps of particles formed due to their own self-gravity as white dots. These clumps are mostly made up of intermediate-sized particles with $\tau_f = [0.1, 1.0]\Omega^{-1}$, which tend to concentrate most effectively (see also Fig. 3). The masses of these clumps are typically of the order of $10^{-3} - 10^{-2} M_{Earth}$ (Gibbons et al. 2014). At this time, the gas density and PV fields are shown in Figs. 6 and 7, respectively. Remarkably, majority of these clumps are formed within the vortices. Consistent with the above case before switching on particle self-gravity (Fig. 3), the particles with $\tau_f = 0.1\Omega^{-1}$ experience clumping in over-dense rings around vortices, whereas larger particles with $\tau_f = 1.0\Omega^{-1}$ in more diffuse vortices with negative and smaller by absolute value PV (curly areas in Fig. 7). As mentioned above, these evolved vortices tend to give rise to higher over-densities in the gas than the density waves do, as evident from Fig. 6 (especially the one in the central-lower region). Thus, irregular, smaller vortices appear to be more efficient at trapping particles than relatively large scale density waves. This suggests that vortical perturbations can be as important as density waves in accumulating solids in self-gravitating discs.

4 SUMMARY AND DISCUSSION

In this paper, we investigated the particle trapping properties of vortices and the potential role they can play in the planet formation process at the early stage of protoplanetary disc life, when most of its interior is dense and cool and self-gravity is a dominant agent governing the dynamics and evolution of the disc. However, mass accretion due to the gravitational instability can raise the temperature and activate the magnetorotational instability in the inner disc (e.g., Zhu et al. 2009, 2010; Rice & Armitage 2009), but this effect is beyond the scope of the present analysis, which focuses on the effects of the gravitational instability only. We used a similar simulation set-up as adopted in our previous work (Gibbons et al. 2012, 2014), but took a smaller simulation domain, which allowed us to capture small-scale vortical structures against a backdrop of larger scale density waves. The large-scale picture of the early stages of planetesimal and planet formation described in the above papers remains unchanged: dust particles accumulate within a quasi-steady gaseous spiral structure produced by a combined effect of disc self-gravity and cooling. The work performed here gives us deeper insight into how smaller scale processes affect the dynamics and evolution of particles in the quasi-steady gravitoturbulence. In this state, the smaller scale turbulent vortical motions (eddies) leave their traces in the evolution of the gas density by producing over-dense regions along with spiral density waves. Particles are accumulated both in crests of density waves and in the anticyclonic irregularly-shaped unsteady vortices. Vortices with small, by absolute value, PV are characterized by higher over-densities than those with larger, by absolute value, PV and consequently the particle concentrations in the former turn out to be accordingly higher, even larger than in the density waves for smaller and intermediate-sized particles (Fig. 3). When the self-gravity of the solid component of the disc is introduced,
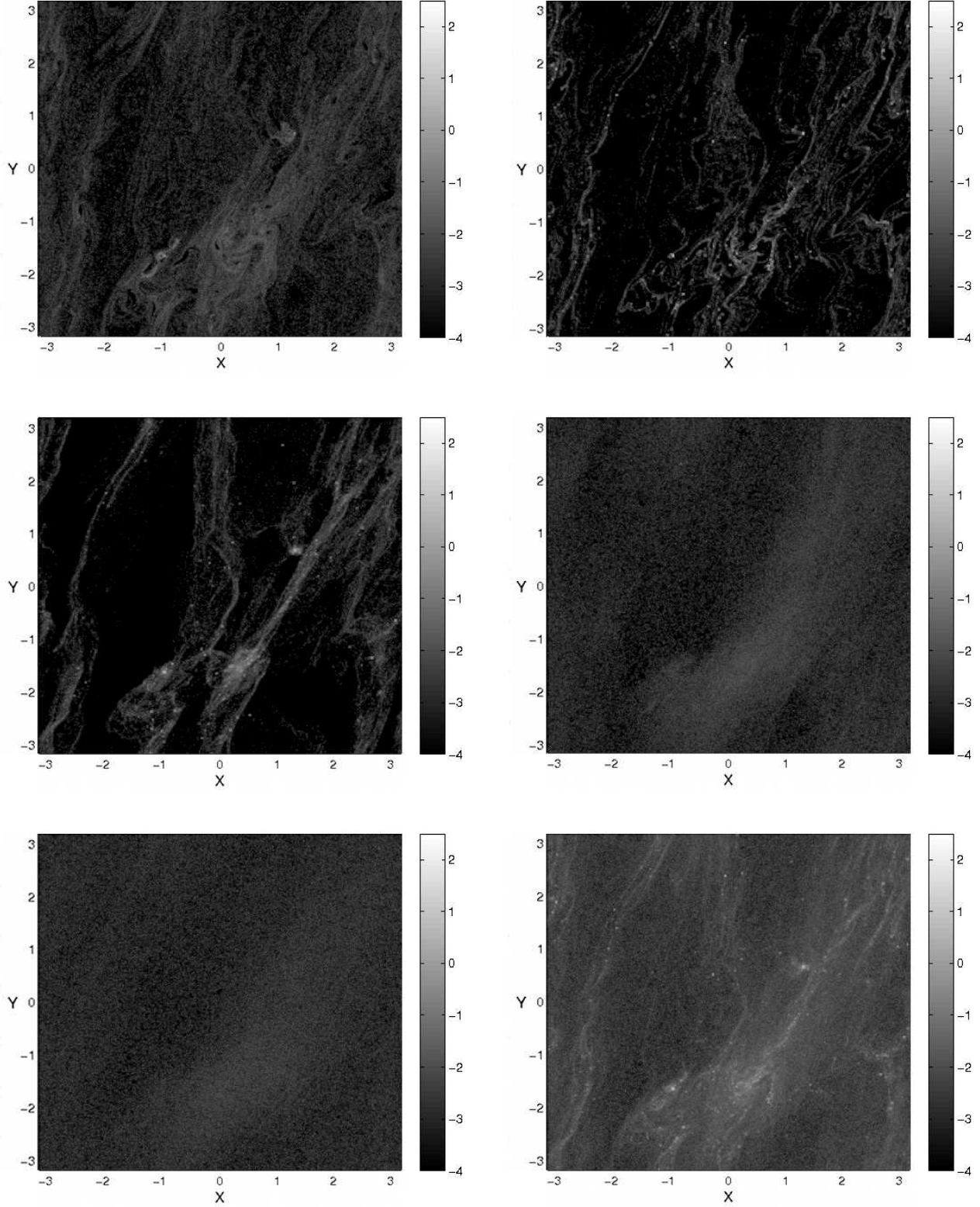
Figure 5. Logarithmic surface density of the individual particle species (in units of its mean $\langle \Sigma_p \rangle = \Sigma_{p0}$) as well as the total surface density (bottom right panel) of the dust at the end of the simulation. Arrangement of the panels according to stopping times is same as in Fig. 3. At this time, the surface density of gas and the PV field are shown, respectively, in Figs. 6 and 7. Only particles with $\tau_f = [0.1, 1.0]\Omega^{-1}$ experience rapid gravitational collapse primarily inside the irregular anticyclonic vortices (compare with Figs. 6 and 7). In such vortices, particles of this size tend to accumulate most effectively and reach relatively high concentrations (see also Fig. 3), leading to the formation of many gravitationally bound particle aggregates, or clumps (white dots) dense enough to survive long after the gas over-density they formed in has dispersed.
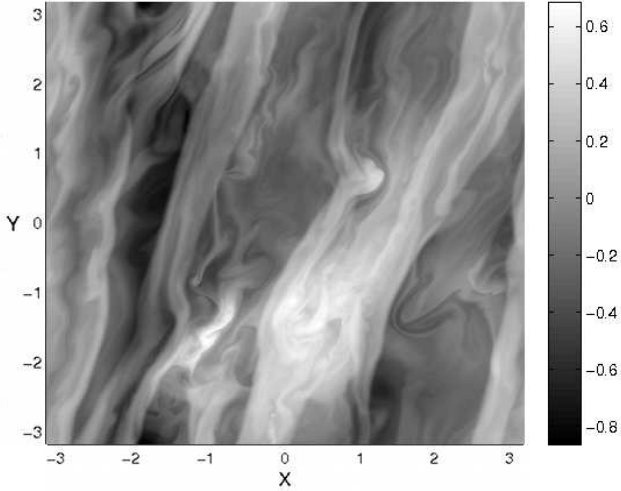
Figure 6. Logarithmic surface density of the gas at the end of the simulation.

Figure 7. PV field at the same time as in Fig. 6, which resembles that in Fig. 2. The colour-map is restricted again to the range $-20 \leqslant I \leqslant 20$. The traces of the PV distribution are clearly seen in the surface density maps of gas and particles at this time depicted in Figs. 6 and 5, respectively.

the particle over-densities that form within these irregular vortices and wave crests rapidly undergo gravitational collapse, forming bound clumps with local densities hundreds of times larger than the typical gas densities within the sheet. Remarkably, the number of clumps formed in the vortices is somewhat larger than that formed in the wave crests (Fig. 5). It is noteworthy that the degree of particle concentration in these structures and hence their clumping property depend on their friction time. We found that small and intermediate-sized dust particles corresponding to friction times comparable to, or less than, the local orbital period of the disc, $\tau_f \leqslant 1.0\Omega^{-1}$, become especially tightly trapped. This suggests that vortical perturbations, which generally are an essential ingredient, together with density waves, in the dynamics of self-gravitating discs can also play an important role in the trapping of dust particles and planetesimal formation at early stages of disc life.

We would like to stress once again that the principal reason for high densities and clumping of particles occurring in this problem is their self-gravity. Here, we have not included particle collisions and one might ask how this effect could modify the results. Johansen et al. (2012) investigated the effect of collisions on the particle dynamics in gaseous discs. They found that collisions, which become more important at high particle concentrations, actually tend to promote particle concentration via damping their rms velocities: the maximum densities of particles including collisions turned out to be more than a factor of three higher compared to those without collisions. The collisions also seem to have no apparent effect on the further clumping/collapse process of these particle concentrations due to their own self-gravity. The masses of the most massive particle clumps (planetesimals) formed are relatively insensitive to the presence or absence of collisions. Based on these results, we anticipate that inclusion of collisions in our problem would not much alter a basic dynamical behavior of particles, although extension of this study with treatment of collisions between numerical super-particles (for example, such as in Johansen et al. 2012) is needed to support this conclusion.

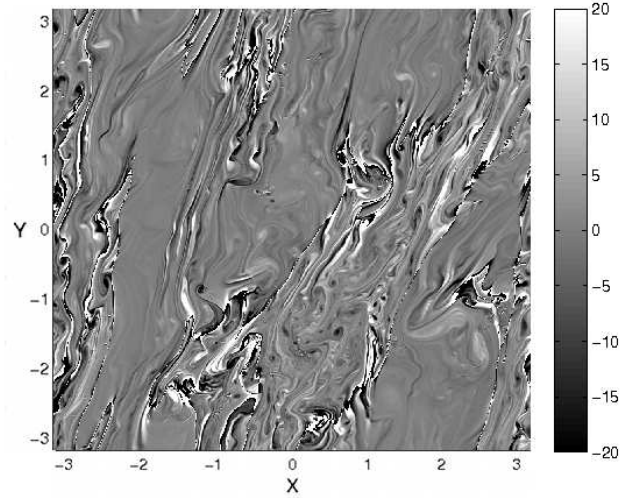In this study, we have considered the simplified case

of a razor-thin (2D) disc with a simple cooling law in order to gain first insight into the effects of vortices on dust particles in the presence of self-gravity. Obviously, for a fuller understanding, three-dimensional (3D) treatment of vortices, with embedded particles, in self-gravitating discs is necessary, which, as far as we are aware, has not been done yet. The dynamics of 3D vortices in non-self-gravitating discs has been investigated in a number of studies (e.g., Barranco & Marcus 2005; Shen et al. 2006; Lesur & Papaloizou 2009; Meheut et al. 2012a; Richard et al. 2013). In the 3D case, in contrast to the 2D one, they are subject to the elliptical instability, which eventually destroys vortices. However, stratification and baroclinic/Rossby wave driving can counteract the elliptical instability, saving vortices from destruction. A self-gravitating 3D disc is clearly stratified in the vertical direction. On the other hand, self-gravity does not favour long-lived regular vortices. But in the 3D case, the effect of self-gravity is somewhat reduced compared to that in the 2D case (e.g., Goldreich & Lynden-Bell 1965; Mamatsashvili & Rice 2010). Thus, it remains to be seen in future numerical studies how the combination of the above factors shapes the dynamics of 3D vortices in self-gravitating discs. When analyzing behaviour of particles in such 3D vortices in self-gravitating discs, one must also take into account the basic effects in the particle dynamics being at work in 3D – sedimentation due to vertical gravity and stir up and clumping of the dust layer due to the Kelvin-Helmholtz and streaming instabilities, respectively (e.g., Youdin & Shu 2002; Johansen et al. 2006; Johansen & Youdin 2007; Johansen et al. 2009; Bai & Stone 2010).

The work presented here expands on the picture of the early stages of planetesimal formation built up by Gibbons et al. (2012, 2014), which still presents an attractive method for the rapid creation of a large reservoir of planetesimals, along with several massive objects of mass $\sim 10^{-2} M_{Earth}$. These objects are then likely to continue

to grow via the traditional core accretion process (e.g., Pollack et al. 1996). Further work, which allows the replacement of large, gravitationally bound accumulations of particles with 'sink' particles, interacting with the disc and with each other, could expand the scope of simulations such as those presented above. This would allow for the subsequent evolution of these planetesimal-sized objects and could proved further insight into how quickly the core accretion process can work in self-gravitating discs.

REFERENCES

Andrews S. M., Williams J. P., 2007, ApJ, 671, 1800
Ataiee S., Dullemond C. P., Kley W., Regaly Z., Meheut H., 2014, A&A, 572, A61
Bai X.-N., Stone J., 2010, ApJ, 722, 1437
Barge P., Sommeria J., 1995, A&A, 295, L1
Barranco J., Marcus P., 2005, ApJ, 623, 1157
Bodo G., Tevzadze A., Chagelishvili G., Mignone A., Rossi P., Ferrari A., 2007, A&A, 475, 51
Bodo G., Chagelishvili G., Murante G., Tevzadze A., Rossi P., Ferrari A., 2005, A&A, 437, 9
Boley A. C., Mejia A., Durisen R., Cai K., Pickett M., D'Alessio P., 2006, ApJ, 651, 517
Boss A. P., 1998, Nature, 393, 141
Brandenburg A., 2003, in Advances in Nonlinear Dynamos, ed. A. Ferriz-Mas & M. Nunez (London: Taylor & Francis), 269
Clarke C.J., 2009, MNRAS, 396, 1066
Cossins P., Lodato G., Clarke C., 2009, MNRAS, 396, 1157
Durisen R. H., Boss A. P., Mayer L., Nelson A. F., Quinn T., Rice, W. K. M., Protostars and Planets V, B. Reipurth, D. Jewitt, and K. Keil (eds.), University of Arizona Press, Tucson, 951, pp., 2007., p.607-622
Eisner J., Hillenbrand L., Carpenter J., Wolf S., 2005, ApJ, 635, 396
Forgan D., Rice W. K. M., Cossins P., Lodato G., 2011, MNRAS, 410, 994
Fu W., Li H., Lubow S., Li S., Liang E., 2014, ApJ, 795, 39
Gammie C. F., 2001, ApJ, 553, 174
Gibbons P. G., Mamatsashvili G. R., Rice W. K. M., 2014, MNRAS, 442, 361
Gibbons P. G., Rice W. K. M., Mamatsashvili G. R., 2012, MNRAS, 426, 1444
Godon P., Livio M., 2000, ApJ, 537, 396
Godon P., Livio M., 1999, ApJ, 523, 350
Goldreich P., Lynden-Bell D., 1965, MNRAS, 130, 97
Guan X., Gammie C., Simon J., Johnson B., 2009, ApJ, 694, 1010
Heinemann T., Papaloizou J. C. B., 2009, MNRAS, 397, 52
Johansen A., Youdin A., Lithwick Y., 2012, A&A, 537, A125
Johansen A., Klahr H., Henning Th., 2011, A&A, 529, A62
Johansen A., Youdin A., Mac Low M.-M., 2009, A&A, 704, L75
Johansen A., Oishi J. S., Mac Low M., Klahr H., Henning Th., Youdin A., 2007, Nature, 448, 1022
Johansen A., Youdin A., 2007, ApJ, 662, 627
Johansen A., Klahr H., Henning T., 2006, ApJ, 643, 1219
Johansen A., Andersen A. C., Brandenburg A., 2004, A&A, 417, 361
Johnson B.M., Gammie C. F., 2005, ApJ, 635, 149
Johnson B. M., Gammie C. F., 2003, ApJ, 597, 131
Klahr H. H., Bodenheimer P., 2006, ApJ, 639, 432
Klahr H., Bodenheimer P., 2003, ApJ, 582, 869
Lesur G., Papaloizou J. C. B., 2010, MNRAS, 513, 60
Lesur G., Papaloizou J. C. B., 2009, A&A, 498, 1
Li H., Colgate S. A., Wendroff B., Liska R., 2001, ApJ, 551, 874
Li H., Finn J. M., Lovelace R. V. E., Colgate S. A., 2000, ApJ, 533, 1023
Lin D. N. C., Pringle J. E., 1990, ApJ, 358, 515
Lin D. N. C., Pringle J. E., 1987, MNRAS, 225, 607
Lin M.-K., 2012a, ApJ, 754, 21
Lin M.-K., 2012b, MNRAS, 426, 3211
Lithwick Y., 2007, ApJ, 670, 789
Lovelace R. V. E., Hohlfeld R. G., 2013, MNRAS, 429, 529
Lovelace R. V. E., Li H., Colgate S. A., Nelson A. F., 1999, ApJ, 513, 805
Lyra W., Lin M.-K., 2013, ApJ, 775, 17
Lyra W., Klahr H., 2011, A&A, 527, 138
Lyra W., Johansen A., Zsom A., Klahr H., Piskunov N. 2009, A&A, 497, 869
Lyra W., Johansen A., Khlar H., Piskunov N., 2008, A&A, 479, 883
Mamatsashvili G. R., Rice W. K. M., 2010, MNRAS, 406, 2050
Mamatsashvili G. R., Rice W. K. M., 2009, MNRAS, 394, 2153
Mamatsashvili G. R., Chagelishvili G. D., 2007, MNRAS, 381, 809
Meheut H., Keppens R., Casse F., Benz W., 2012a, A&A, 542, 9
Meheut H., Meliani Z., Varniere P., Benz W., 2012b, A&A, 545, 134
Meheut H., Casse F., Varniere P., Tagger M., 2010, A&A, 516, 31
Paardekooper S.-J., 2012, MNRAS, 421, 3286
Paardekooper S.-J., Lesur G., Papaloizou J. C. B., 2010, ApJ, 725, 146
Petersen M. R., Julien K., Stewart G. R., 2007, ApJ, 658, 1236
Pollack J. B., Hubickyj O., Bodenheimer P., Lissauer J., Podolak M., Greenzweig Y., 1996, Icarus, 124, 62
Raettig N., Lyra W., Klahr H., 2013, ApJ, 765, 115
Rafikov R. R., 2005, ApJ, 621, L69

Regaly Zs., Juhasz A., Sandor Zs., Dullemond C. P., 2012, MNRAS, 419, 1701

Rice W. K. M., Armitage P. J., Mamatsashvili G. R., Lodato G., Clarke C. J., 2011, MNRAS, 418, 1356

Rice W. K. M., Mayo J. H., Armitage P. J., 2010, MNRAS, 402, 1740

Rice W. K. M., Armitage P. J., 2009, MNRAS, 396, 2228

Rice W. K. M., Lodato G., Pringle J. E., Armitage P. J., Bonnell I. A., 2006, MNRAS, 372, L9

Rice W. K. M., Lodato G., Pringle J. E., Armitage P. J., Bonnell I. A., 2004, MNRAS, 355, 543

Rice W. K. M., Armitage P. J., Bate M. R., Bonnell I. A., 2003, MNRAS, 338, 227

Richard S., Barge P., Le Dizes S., 2013, A&A, 559, 30

Shen Y., Stone J. M., Gardiner T. A., 2006, ApJ, 653, 513

Umurhan O. M., Regev O., 2004, A&A, 427, 855

Youdin A., Johansen A., 2007, ApJ, 662, 613

Youdin A., Shu F., 2002, ApJ, 580, 494

Zhu Z., Stone J. M., Rafikov R. R., Bai X.-N., 2014, ApJ, 785, 122

Zhu Z., Hartmann L., Gammie C., Book L., Simon J., Engelhard E., 2010, ApJ, 713, 1134

Zhu Z., Hartmann L., Gammie C., 2009, ApJ, 694, 1045

APPENDIX A: RESOLUTION TEST

To investigate the effects of resolution on the dynamics of vortices in the presence of self-gravity, we ran simulations for a domain with half size, $L_x/2 = L_y/2 = 10/\pi$ (in units of H, initial $Q = 1$) at three different resolutions $N_x \times N_y = 256 \times 256, 512 \times 512, 1024 \times 1024$, including the same number of particles and starting with the same initial conditions as in the paper. This is equivalent to running the fiducial model with $L_x = L_y = 20/\pi$ considered in this work at doubled resolutions 512×512, 1024×1024 and 2048×2048, respectively, since the corresponding grid cell sizes, $\delta x = L_x/N_x = 0.0124, 0.0062, 0.0031$ would be the same in both cases. So far as numerical convergence is concerned, grid cell size is a central length-scale, since measuring various physical lengths of the system against it allows us to find out whether a simulation is resolved. Therefore, due to the same grid cell sizes, a resolution study we do for the half-size model also establishes whether vortices in the fiducial model are sufficiently resolved.

In the quasi-steady state, the PV fields from all these three runs at the same time are shown in Fig. A1. These fields, being at different resolutions, display essentially identical structures, indicating that they are resolved. To put this conclusion on more quantitative grounds, as in Johnson & Gammie (2005), we consider the autocorrelation function for the fluctuating part of PV, $\delta I = I - \langle I \rangle$, given by

$$\zeta(\mathbf{\Delta x}) = \langle \delta I(\mathbf{x}) \delta I(\mathbf{x} + \mathbf{\Delta x}) \rangle,$$

where the angle brackets denote average over the whole domain. Figure A2 shows the autocorrelation functions corresponding to the PV fields in Fig. A1. They do appear similar and their cores have nearly an elliptical shape with minor and major principal axis. Following the method of Guan et al. (2009), we calculated related correlation lengths
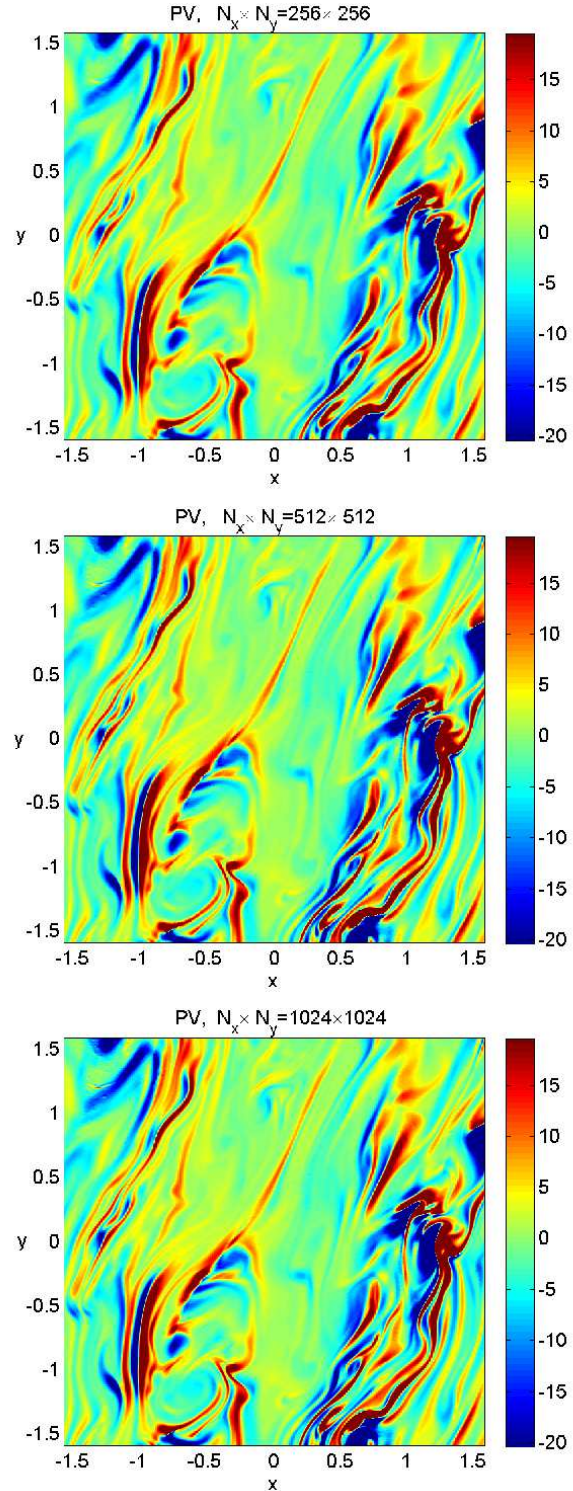

Figure A1. PV field for the half size domain at different resolutions in the quasi-steady state at the same time (colour online).

along these axes by

$$\lambda_{min} = \frac{1}{\zeta(0)} \int_0^\infty \zeta(l\hat{\mathbf{x}}_{min})dl, \quad \lambda_{maj} = \frac{1}{\zeta(0)} \int_0^\infty \zeta(l\hat{\mathbf{x}}_{maj})dl,$$

where l is the distance from $\mathbf{\Delta x} = 0$ along the principal axes given by the unit vectors $\hat{\mathbf{x}}_{min}$ and $\hat{\mathbf{x}}_{maj}$. These correlation

lengths can be used as a measure for the typical size of the PV structures.

The smallest correlation lengths along the minor axis are $\lambda_{min} = 0.088, 0.079, 0.077$, for the lowest, intermediate and highest resolution runs, respectively. The ratios of the minimum correlation length to the grid cell size at these resolutions are, respectively, $\lambda_{min}/\delta x = 7.1, 12.7, 24.8$. This ratio increases with resolution which serves as an indication for convergence and, as a matter of fact, implies that the vortices (eddies) can be considered to be sufficiently resolved in the fiducial model which has $\delta x = 0.0062$. In our previous papers Gibbons et al. (2012, 2014), the domain size is $L_x = L_y = 80/\pi$ and resolution 1024×1024 for the same other parameters, giving $\delta x = 0.0249$ and hence $\lambda_{min}/\delta x < 3.5$. Thus, although this resolution is quite suitable to resolve larger scale density waves in those studies, it is still coarse to detect and examine vortical structures at such larger domain sizes in contrast to that at four times smaller domain size used in the present paper.
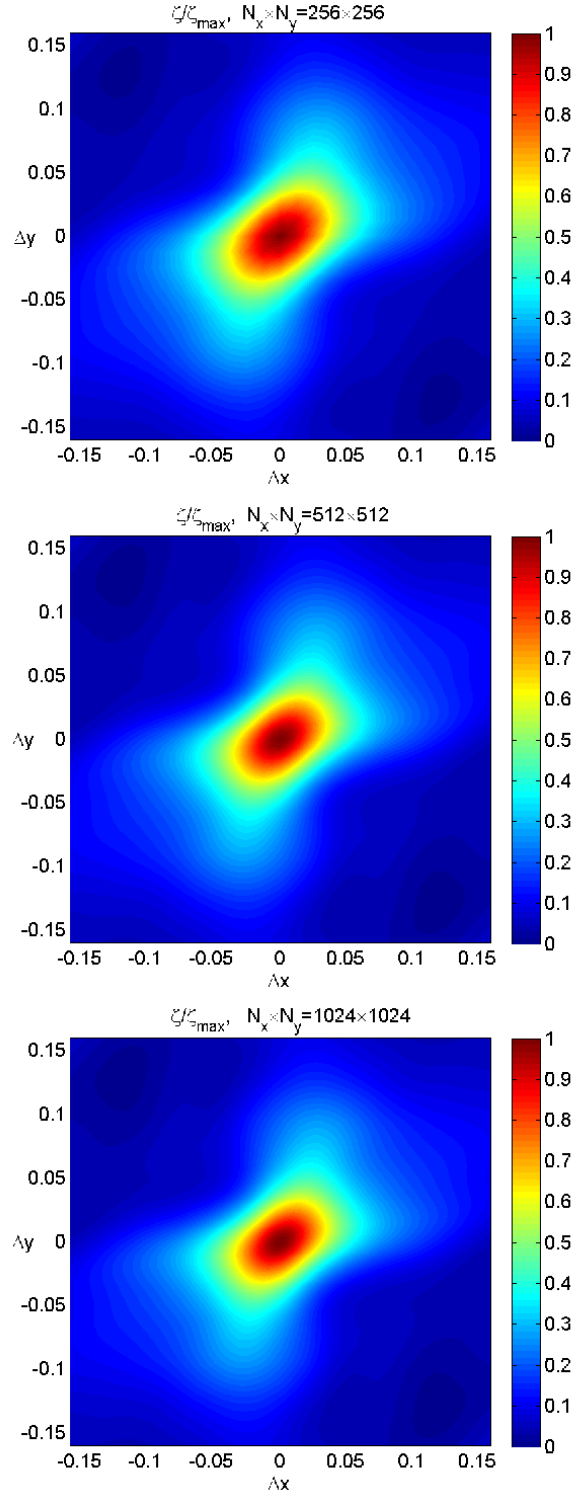

Figure A2. Normalized autocorrelation function, ζ/ζ_{max}, where $\zeta_{max} = \zeta(0)$, corresponding to the PV in Fig. A1 at different resolutions (colour online).